Semiparametric Estimation of Spectral Density with Irregular Observations

Hae Kyung Im, Michael L. Stein, and Zhengyuan Zhu[*]

Abstract

We propose a semiparametric method to estimate spectral densities of isotropic Gaussian processes with scattered data. The spectral density function (Fourier transform of the covariance function) is modeled as a linear combination of B-splines up to a cutoff frequency and, from this point, a truncated algebraic tail. We calculate an analytic expression for the covariance function and tackle several numerical issues that arise when calculating the likelihood. The parameters are estimated by maximizing the likelihood using the simulated annealing method. Our method directly estimates the tail behavior of the spectral density, which has the biggest impact on interpolation properties. The use of the likelihood in parameter estimation takes fully into account the correlations between observations. We compare our method with a kernel method proposed by Hall et al. (1994) and a parametric method using the Matérn model. Simulation results show that our method outperforms

[*]Hae Kyung Im is Research Associate, CISES, the University of Chicago, Chicago, IL 60637 (E-mail: haky@uchicago.edu). Michael L. Stein is Professor, Department of Statistics, the University of Chicago, Chicago, IL 60637. Zhengyuan Zhu is Assistant Professor, Department of Statistics and Operations Research, the University of North Carolina at Chapel Hill, Chapel Hill, NC 27599 (E-mail: zhuz@email.unc.edu).

the other two by several criteria. Application to rainfall data shows that our method outperforms the kernel method.

Key words: covariance function; maximum likelihood; B-spline; kriging;

1   Introduction

Estimation of the covariance structure of physical processes observed at a finite set of locations is fundamental to understand the behavior of such processes and to interpolate to locations where measurements are not available. Kriging, an interpolation method widely used by the geophysical community, is based on the knowledge of the covariances between observed and interpolated locations.

We will concentrate on Gaussian isotropic processes, which are invariant under all rigid motions. Under this assumption, the covariance of the process at two locations only depends on the distance between them, so a covariance function on $\mathbb{R}^+$ fully describes the second order properties of the process. This function has to be positive definite in order to ensure that the variance of any linear combinations of values of the process at various locations is positive. The most common solution to this problem is to restrict the estimation to parametric forms that are proven to be positive definite.

There has been some work in using nonparametric methods or a broad class of positive definite functions based on the spectral representation of covariance functions. Before describing these methods some review of positive definite functions is in order. Bochner's Theorem (Yaglom, 1987) states that a function is continuous and positive definite if and only if it is the Fourier transform of a positive bounded measure on $\mathbb{R}^d$, i.e.,

$$C(\mathbf{x}) = \int_{\mathbb{R}^d} \exp(i\mathbf{w}\mathbf{x}) F(\mathbf{dw}). \tag{1}$$

For isotropic processes (1) can be reduced to a one-dimensional integral

$$C(r) = 2^{(d-2)/2}\Gamma(d/2) \int_0^\infty (ru)^{-(d-2)/2} J_{(d-2)/2}(ru) dG(u), \tag{2}$$

where $G(u) = \int_{|\mathbf{w}|<\mathbf{u}} dF(\mathbf{dw})$ is a bounded positive measure on $\mathbb{R}$, $\Gamma(\cdot)$ is the Gamma function, and $J_\nu(\cdot)$ is the Bessel function of the first kind of order ν (Abramowitz and Stegun (1965), pg.355).

Shapiro and Botha (1991) proposed using a finite discrete measure with nodes placed at $t_1, ..., t_n$ so that the integral in (2) is reduced to a finite sum:

$$\tilde{C}(r) = \sum_{j=1}^m p_j \Omega_d(t_j h), \tag{3}$$

where the p_j's are positive and $\Omega_d(x) = \left(\frac{2}{x}\right)^{(d-2)/2} \Gamma\left(\frac{d}{2}\right) J_{(d-2)/2}(x)$. For a random field Z on $\mathbb{R}^d$, they use a raw covariogram estimate given by

$$\hat{C}(h) = \frac{1}{N(h)} \sum_{N(h)} (Z(\mathbf{x}_i) - \bar{Z})(Z(\mathbf{x}_j) - \bar{Z}), \tag{4}$$

where $\mathbf{x}_1, \ldots, \mathbf{x}_n$ are observation sites, $\bar{Z}$ is the average of the observations, the sum in (4) runs over all pairs of observations that are approximately distance h apart, and $N(h)$ is the total number of such pairs. They estimate the values of p_j by minimizing the mean squared difference between the raw covariogram estimate at different lags and their estimator, with positivity constraint.

Genton and Gorsich (2002) follow this idea but propose using the zeros of the Bessel functions as the nodes of the discrete measure and show that their method is computationally simpler, needs fewer nodes, and does not show spurious oscillations. A problem with this choice of nodes is that these numbers are nondimensional. It is not clear what scale should be used to translate these nodes into nodes in the frequency domain (which have dimension 1 / unit of distance). Although not totally explicit, they seem to propose using $1/r_{\max}$ as their scale. This would mean that if we

added an additional observation at distance 1.5 $r_{\max}$ from the most distant existing observation, then the nodes would be shifted by a factor of 1.5 in the frequency domain. This behavior seems problematic.

Hall et al. (1994) propose using a kernel estimator for a preliminary covariogram estimate and, in order to ensure positive definiteness, they propose Fourier transforming the kernel estimator, setting the negative values to zero and Fourier transforming back to the spatial domain. For $d = 2$, denoting $\hat{Z}_{ij} = (Z(\mathbf{x}_i) - \bar{Z})(Z(\mathbf{x}_j) - \bar{Z})$, h_{ij} the distance between the observations Z_i and Z_j, K a kernel function (a positive symmetric probability density), and δ the bandwidth, the first step estimator of the covariogram is

$$\tilde{C}(h) = \frac{\sum_{i,j} \hat{Z}_{ij} K(\frac{h - h_{ij}}{\delta})}{\sum_{i,j} K(\frac{h - h_{ij}}{\delta})}. \tag{5}$$

The final estimate of the covariogram is

$$\bar{C}(h) = \int_0^\infty \left(\int_0^\infty \tilde{C}(x) x J_o(wx) dx \right)_+ w J_o(wh) dw, \tag{6}$$

where the subscript $+$ means to take the positive part of the expression. We will call this function the kernel estimator of the covariance function.

All three methods use the raw covariogram as the basis for estimation, which does not take into account the correlation between different $\hat{Z}_{ij}$'s. Furthermore, it is well known that the high frequency properties of the spectral density determine the performance of interpolation procedures (Stein (1999), pg.65). None of the above methods gives proper consideration to the tail properties.

We propose a flexible family of models for the spectral density that is a linear combination of B-splines of order 4 (cubic splines) up to a cutoff frequency w_t and an algebraically decaying tail from w_t to infinity. We use positive coefficients for the B-splines, which ensure positiveness of the spectral density and, as a consequence, positive definiteness of the covariance function. Assuming the process is well described

by a Gaussian random field, we find the parameters that maximize the likelihood. This method estimates the tail property of the spectral density in an explicit way. It does exclude exponential decay of the tail. However, we consider this restriction to be beneficial, since such a fast decay would imply an unrealistically smooth process (Stein (1999), pg.29, Stein (2002)). It also excludes oscillatory tails such as $w^{-\gamma}\cos^2 w$, which are generally undesirable (Stein (1999), pg.67-8 and Stein (2002)). Additionally, through the use of likelihood, our method takes fully into account all the correlations between observations. This is, to the extent of our knowledge, the first work that uses a likelihood approach for scattered spatial data without a parametric model.

In section 2 we present our model and the methodology to estimate the covariance function. Section 3 describes how to deal with the numerical challenges that arise when calculating the likelihood. In section 4 we describe several performance measures and, via a simulation study, compare our method with a parametric method using the Matérn model and the nonparametric kernel method in Hall et al. (1994). Section 5 compares the three methods using a rainfall dataset. The simulation study shows that our method is substantially better than the kernel method and often better than using the Matérn model. A real data example also shows that our method outperforms the kernel method. Section 6 summarizes the paper and discusses possible further work.

2   Methodology

We assume the observations come from realizations of a Gaussian random field whose value at location x is of the form

$$Z(\mathbf{x}) = \mathbf{m}(\mathbf{x})^T \boldsymbol{\beta} + \epsilon(\mathbf{x}), \tag{7}$$

where $\mathbf{m}(\mathbf{x})$ is a known vector valued function, $\boldsymbol{\beta}$ is a vector of unknown coefficients, ϵ has mean 0 with covariance function $C(\epsilon(\mathbf{x}), \epsilon(\mathbf{y})) = C_{\boldsymbol{\theta}}(|\mathbf{x} - \mathbf{y}|)$, and $\boldsymbol{\theta}$ is the vector of unknown parameters of the covariance function.

2.1 The splines+tail (S+T) model and the Matérn model for the spectral density

Let any $f(w)$ be the spectral density of $\epsilon(\mathbf{x})$ in (7), our S+T model can be written as

$$f_{\boldsymbol{\theta}}(w) = \sigma^2 \sum_{i=-1}^{l+1} b_i B_i(w) \mathbf{1}_{[0, w_t]}(w) + C_f \left(\frac{w_t}{w}\right)^{\gamma} \mathbf{1}_{(w_t, \infty)}(w), \qquad (8)$$

where $\mathbf{1}_A(w)$ is an indicator function of value one if $w \in A$, and zero otherwise. The B_is are B-splines of order 4 (See Appendix A for a brief description and references) with node sequence $(w_0, ..., w_l)$ on the interval $[0, w_t]$, with w_t the threshold frequency. The sum goes from -1 to $l + 1$ in order to include all B-splines that have support on the interval $[0, w_t]$. We chose order 4 because of the flexibility that cubic splines give to represent a wide range of smooth functions. B-splines of other orders could be used with minor adjustments. We require the spectral density to be continuous and have continuous derivative at w_t. The constant C_f is chosen to achieve continuity at w_t; more explicitly, $C_f = \sigma^2 \sum_{i=-1}^{l+1} b_i B_i(w_t)$. The coefficients of the B-splines are constrained to be positive except for b_{l+1}, which is chosen so that the derivative of $f_{\boldsymbol{\theta}}(w)$ is continuous at w_t. It is shown in Appendix D that the function is still positive. Restricting the coefficients to be positive is a simple way of ensuring positivity of the function.

To specify a S+T model, we first need to determine the number and location of the nodes for the B-splines. In this paper, we restrict the B-splines to have uniformly distributed nodes between 0 and w_t, i.e., given the number of nodes $(l + 1)$ and the cutoff frequency (w_t), we place the nodes at locations iw_t/l for $i = -1, 0, ..., l, l + 1$.

Conditional on knowing the number of nodes, the parameter $\boldsymbol{\theta}$ of our S+T model includes smoothness parameter γ, sill σ^2, cutoff frequency w_t, and the coefficients of B-splines (b_i for $i = 0, ..., l$). The coefficients b_{-1} and b_{l+1} determine the derivatives of the function at the end points. We chose b_{-1} to equal b_1 in order to make $f'(0) = 0$ and b_{l+1} to be such that the derivative of the function is continuous at w_t (See Appendix C).

Let us briefly describe the Matérn model in order to compare it to our model. This class is considered to be a sensible model for a wide range of processes arising in environmental problems (Stein, 1999; Handcock and Wallis, 1994). With only three easily interpretable parameters (σ^2, ϕ and ν), the Matérn class allows considerable flexibility in the type of processes it can represent. The parameter σ^2 is simply the variance of the process at a given location, ϕ is the inverse range parameter, and ν is a measure of the smoothness of the process. The spectral density of the Matérn class has the form

$$f(w) = \frac{\sigma^2 \lambda(\phi, \nu)}{(\phi^2 + w^2)^{\nu + d/2}} \tag{9}$$

with $\lambda(\phi, \nu) = \frac{\Gamma(\nu + d/2)}{\pi^{d/2} \Gamma(\nu)} \phi^{2\nu}$ such that the variance, $C(0)$, is σ^2. At high frequencies both the Matérn and our S+T model approach zero at the rate $1/w^\gamma$, with $\gamma = 2\nu + d$. In the simulation studies, we will use ν as the parameter for the S+T model.

2.2 Compute covariance function using the Hankel transform

The covariance function can be calculated from the spectral density $f_{\boldsymbol{\theta}}(w)$ by applying (2) for $d = 2$:

$$C_{\boldsymbol{\theta}}(r) = 2\pi \int_0^\infty w J_o(rw) f_{\boldsymbol{\theta}}(w) dw. \tag{10}$$

The transform in (10) is called the Hankel transform of order 0. A function $f_{\boldsymbol{\theta}}(w)$ in the S+T family is a linear combination of B-splines and an algebraic tail; the Hankel transform of both components can be calculated analytically. The Hankel transform

of B-splines requires calculating two Bessel functions of the first kind of orders 1 and 2 and two Struve functions of orders 1 and 2 (Abramowitz and Stegun (1965), pg.495) for each node. The computation of this part is straightforward albeit moderately time consuming. See Appendix B for details. The Hankel transform of the truncated algebraic tail is

$$\int_{w_t}^{\infty} w^{1-\gamma} J_o(wr) dw$$
$$= r^{\gamma-2} \left(\frac{\gamma\Gamma(-\gamma/2)}{2^\gamma\Gamma(\gamma/2)} + \frac{(w_t r)^{2-\gamma} {}_1F_2(1-\gamma/2; 1, 2-\gamma/2; -(rw_t)^2/4)}{\gamma-2} \right), \tag{11}$$

where $_1F_2(a; b, c; z)$ is a generalized hypergeometric function with series representation $\sum_{k=0}^{\infty} \frac{(a)_k}{(b)_k(c)_k} \frac{z^k}{k!}$. Here $(\cdot)_k$ represents the Pochhammer's symbol (Abramowitz and Stegun (1965), pg.256), which is defined by $(z)_0 = 1$ and $(z)_k = z(z+1)(z+2)...(z+n-1) = \frac{\Gamma(z+n)}{\Gamma(z)}$.

Several features make the Hankel transform of the tail (11) numerically hard to compute. First, there is no easy way of evaluating this hypergeometric function accurately without resorting to summing a large number of terms of its series expansion, which can lead to severe numerical errors. Second, the Γ function is infinite when the argument is a negative integer, and we have no reason to exclude negative integer values for $-\gamma/2$. Third, the first term, $\gamma\Gamma(-\gamma/2)/2^\gamma\Gamma(\gamma/2)$, is the limit of the second term, $(w_t r)^{2-\gamma} {}_1F_2(1-\gamma/2; 1, 2-\gamma/2; -(rw_t)^2/4)/\gamma-2$, as $rw_t \to \infty$, so in the case where rw_t is large we need to take the difference of two very similar numbers.

The first problem is addressed by using arbitrary precision arithmetic libraries (code downloaded from http://www.mpfr.org/). For the second problem, we note that the divergence of the Γ function is compensated by the divergence of one of the terms of the series expansion of the hypergeometric function. When $\gamma/2$ is an integer, we use an asymptotic expansion of the Γ function when the argument is close to $-\gamma/2$, and subtract it from the series expansion of the hypergeometric function. Only one term in each series expansion diverges as the arguments approaches $-\gamma/2$, and we

8

get a modified series expansion for the difference between the two terms, which can be computed in the same fashion as the hypergeometric function, i.e., by adding the series until convergence is achieved and using arbitrary precision libraries to avoid numerical errors. The final expression for the tail integral when $\gamma/2 = n+1$ is

$$
\begin{aligned}
&\int_{w_t}^{\infty} w^{1-\gamma} J_o(wr)dw \\
&= r^{2n} \frac{\log(2) - \log(rw_t) + \psi(n+1)}{(-4)^n n!^2} + \frac{w_t^{2n}}{2n} \sum_{k=0, k \neq n}^{\infty} \frac{-n}{-n+k} \frac{(-(rw_t)^2/4)^k}{k!^2},
\end{aligned}
\tag{12}
$$

where $\psi(n)$ is the digamma function (Abramowitz and Stegun (1965), pg.258), which for positive integer arguments can be evaluated as $\sum_{k=1}^{n-1} \frac{1}{k} - \gamma_{eg}$,where $\gamma_{eq} = 0.577216...$ is the Euler's constant. The details are given in Appendix E.

To solve the third problem of subtracting two very similar numbers, we again use an asymptotic expansion of the hypergeometric function, whose leading term is $\frac{\gamma \Gamma(-\gamma/2)(\gamma-2)}{/} \left(2^\gamma \Gamma(\gamma/2)(rw_t)^{2-\gamma}\right)$. As a result, we are left with an expression that directly calculates the difference. See details in Appendix F. For large values of rw_t the Hankel transform of the truncated tail is approximated by

$$
\begin{aligned}
&\int_{w_t}^{\infty} w^{1-\gamma} J_o(wr)dw \\
&\approx \left(\frac{\cos(rw_t) - \sin(rw_t)}{\sqrt{\pi}(rw_t)^{\gamma-\frac{1}{2}}} - \frac{\left(-15 + 16\gamma + 128\gamma^2\right)(\cos(rw_t) - \sin(rw_t))}{128\sqrt{\pi}(rw_t)^{\gamma+\frac{3}{2}}} \right. \\
&\quad \left. + \frac{(-3 + 8\gamma)(\cos(rw_t) + \sin(rw_t))}{8\sqrt{\pi}(rw_t)^{\gamma+\frac{1}{2}}} + \dots \right) r^{\gamma-2}.
\end{aligned}
\tag{13}
$$

The approximation (13) also apply when $\gamma/2$ is an integer.

2.3   Likelihood based parameter estimation

Let $\mathbf{Z} = (Z(\mathbf{x}_1), ..., Z(\mathbf{x}_n))^T$ be our observation and $\mathbf{M} = (\mathbf{m}(\mathbf{x}_1)...\mathbf{m}(\mathbf{x}_n))^T$. Under model (7), the log-likelihood has the form

$$
l(\boldsymbol{\theta}, \boldsymbol{\beta}; \mathbf{Z}) = -\frac{1}{2} \log|\det\boldsymbol{\Sigma}_{\boldsymbol{\theta}}| - \frac{1}{2}(\mathbf{Z} - \mathbf{M}\boldsymbol{\beta})^T \boldsymbol{\Sigma}_{\boldsymbol{\theta}}^{-1}(\mathbf{Z} - \mathbf{M}\boldsymbol{\beta}) - \frac{n}{2}\log(2\pi),
\tag{14}
$$

9

where $\mathbf{\Sigma}_{ij} = C_{\boldsymbol{\theta}}(|\mathbf{x}_i - \mathbf{x}_j|)$ can be computed using (10) and (8). If the mean parameter $\boldsymbol{\beta}$ can be assumed known, one can estimate the parameter $\boldsymbol{\theta}$ of the S+T model by maximizing (14). When $\boldsymbol{\beta}$ is unknown, $\boldsymbol{\theta}$ can be estimated by maximizing the following restricted likelihood, REML (Stein (1999), pg.170 and McCullagh and Nelder (1989), section 7.2), which can be calculated by (ignoring an additive constant):

$$rl(\boldsymbol{\theta}|;\mathbf{Z}) = -\frac{1}{2}\log|\det\mathbf{\Sigma}_{\boldsymbol{\theta}}| - \frac{1}{2}\log|\det\mathbf{W}| - \frac{1}{2}\mathbf{Z}^T(\mathbf{\Sigma}_{\boldsymbol{\theta}}^{-1} - \mathbf{\Sigma}_{\boldsymbol{\theta}}^{-1}\mathbf{M}\mathbf{W}^{-1}\mathbf{M}^T\mathbf{\Sigma}_{\boldsymbol{\theta}}^{-1})\mathbf{Z} \quad (15)$$

where $\mathbf{W} = \mathbf{M}^T\mathbf{\Sigma}_{\boldsymbol{\theta}}^{-1}\mathbf{M}$.

3 Numerical Implementation

The need for high computational speed forced us to discretize some of the parameters (smoothness and cutoff frequencies), so the usual continuous optimization routines are not applicable, and we use the simulated annealing method (Section 3.1) to maximize the likelihood.

The number of nodes can be determined using some model selection criteria. We use Akaike Information Criterion, which penalizes large number of parameters. We fix the number of nodes l and optimize using simulated annealing as described in 3.1. We repeat this for a few different values for l and choose the one that has smallest AIC. We compared the performance of Akaike Information Criterion (AIC, Akaike (1974)) and Bayes information criterion (BIC, Schwarz (1978)). Our simulation results indicate that AIC is more likely to select the correct number of nodes when the data are simulated using the S+T model, and the prediction performance using AIC is also slightly better than BIC for all the models we used for simulation. We use AIC to select nodes in all the simulation studies presented in section 4 and in the application to rainfall data in section 5.

3.1 Simulated Annealing

We implemented the maximization using the simulated annealing method (Givens and Hoeting, 2005). This method is based on the way a physical system finds its minimum energy state when it is first heated to high temperature and then cooled down slowly to zero temperature. In our problem, the energy to be minimized is the negative of the log-likelihood function. One starts with an initial value of the parameters and calculates the energy. New values of the parameters are drawn from a proposal distribution and the new energy is calculated. If the new energy is lower than the previous one, the parameters get updated with the new values. If the new energy is higher than the initial energy, the new parameters are accepted with probability $\exp(-(E_f - E_i)/T)/(1 + \exp(-(E_f - E_i)/T))$, where E_i and E_f are the initial and final energies and T is the temperature. This helps keep the system from being trapped in local minima. These steps are repeated several times, after which the temperature is lowered and the same procedure is followed until the temperature is close to 0.

We have noticed that the convergence depends on the starting values of the parameters, most notably on the threshold frequency w_t. We use three different starting values of w_t ($1/r_{\min}$, $1/r_{\max}$, and the average of the two), and choose the estimated parameters that have the largest likelihood. We start by fitting a Matérn model and using the estimated sill (σ) and smoothness (ν) as starting values for the optimization. The initial values for the coefficients of the B-Splines are set to be constant 1 at all nodes. Since we normalize the spectral density so that it yields variance σ^2, the overall scale of the coefficients is not relevant.

The proposal distribution for the coefficients of the B-splines is a mixture of two lognormal distributions, one with mean parameter zero and variance parameter one, and the other one with mean centered at the initial value and variance 0.1. The

proposal distribution for the sill is also a mixture of lognormals, one with mean given by the sample variance of the observations and variance 1, and the other one centered at the initial value with variance 0.1. These numbers were chosen so that the convergence was satisfactory. We let w_t take 100 discrete values between $1/r_{\max}$ to $1/r_{\min}$. The proposal was a mixture of two uniform distributions, one that ranges over all 100 values, and the other one centered at the previous value with a range that is 10% of the whole range. Likewise, we let the smoothness parameter take 100 discrete values between 0.05 and 5. Larger values of smoothness give rise to almost singular covariance matrices. The proposal was also a mixture of uniforms, one centered at the previous value with a range that is 10% of the total range, and the other one over the whole range.

Several cooling schedules were tested. The one that gave slightly better convergence was one that updated the temperature in each step according to $T_i = \frac{T_{i-1}}{1+aT_{i-1}}$ with $a = 30$ and $T_0 = 1000$. We stopped after 10000-20000 iterations, after which no changes in parameters occurred. Each optimization took around 2-5 minutes on a Linux machine with dual AMD Opteron™ processors and 2Gb of memory.

3.2   Tabulation of Hankel transforms

To speed up the computation of the Hankel transforms of the truncated tail, we resort to some further approximations and shortcuts. We calculated the covariance function for $n_r = 100$ equispaced values between $r_{\min}$ and $r_{\max}$ and interpolated using cubic spline interpolation for distances between these points. Also, we restricted the values of the threshold frequency w_t and the power of the tail γ to $n_w = 100$ and $n_\gamma = 100$ discrete values. Namely, $w_t(j) = \frac{1}{r_{\max}} + \frac{j}{n_w}\left(\frac{1}{r_{\min}} - \frac{1}{r_{\max}}\right)$ and $\gamma(j) = 2 + 2\left(0.05 + \frac{j}{n_\gamma}(5 - 0.05)\right)$.

The Hankel transform of the truncated tail, $t(i, j, k) = \int_{w_t(k)}^{\infty} w^{1-\gamma(j)} J_o(wr(i))dw,$

was tabulated into an array of dimensions $n_r \times n_\gamma \times n_w = 100 \times 100 \times 100$. The Hankel transform of piecewise polynomials of the form $\mathbf{1}_{[w_i, w_{i+1})}(w - w_i)^m$ for $m = 0, 1, 2$, and 3 were tabulated into an array of dimensions $l \times 4 \times n_r \times n_w = l \times 4 \times 100 \times 100$, where l is the number of polynomial pieces used in the representation of the spectral density. In order to take advantage of this tabulation at the time of calculating the transform, we converted the splines $S(w)$ (linear combination of B-splines) into a piecewise polynomial form

$$S(w) = \sum_{i=0}^{l} \sum_{j=0}^{3} a_{ij} \mathbf{1}_{[w_i, w_{i+1})}(w - w_i)^j. \tag{16}$$

Hence the Hankel transform was reduced to multiplying the tabulated values by the corresponding coefficients.

The frequency thresholding in the tabulation is unlikely to have an effect in the results since in all the simulations the estimated cutoff frequency was about one order of magnitude smaller than the maximum tabulated value.

4 Simulations

We first simulated Gaussian random fields with mean zero and various covariance functions and estimated the spectral density using the S+T family of functions. For comparison purposes, we also estimated the covariance function using the Matérn model as well as the kernel method proposed by Hall et al. (1994). The locations were chosen to be where the National Acid Deposition Program sites are situated. We used a total of 63 sites that are shown in Figure 1. The smallest distance between sites is 14 km, the largest distance is 2000 km, and the median distance is 802 km. For simplicity, we use chordal distance and ignore the fact that the surface is spherical.

The covariance models we used to simulate the data are Matérn, polynomial

Matérn, S+T, and spectral exponential. Polynomial Matérn is a family of spectral density which is the product of Matérn spectral density and a positive polynomial, $f(w) = ((w-u)^2 + v^2)((w+u)^2 + v^2)/(a^2 + w^2)^{\nu+d/2}$. This function is positive on $\mathbb{R}^+$, thus a valid spectral density. The spectral density of the spectral exponential model has the form $f(w) = \exp(-w/\phi)$, which should not be confused with the exponential correlation function that belongs to the Matérn family and is exponential in the spatial domain. In the simulation study we set $\phi = w_t$. Matérn, S+T and polynomial Matérn share the same high frequency behavior, namely, $1/\omega^\gamma$. The spectral exponential model has a much faster decay and has analytic realizations of the process. Though we do not consider this type of behavior to be reasonable for modeling natural physical processes, it is included here to test the method.

Each simulation includes 200 independent realizations of a Gaussian random field at 63 locations, totaling 12,600 observations with the given covariance functions. The covariance matrix corresponding to this type of datasets is block diagonal, which allows us to have a large number of observations (so that the parameters can be estimated well) while keeping the computational load at a manageable level. For each simulation, the ML parameters for S+T and Matérn models were estimated. Also the kernel estimate of the covariance function was calculated.

In order to assess the performance of each method, we look at the following quantities.

- Parameter values: When the true model and the model used to estimate the covariance functions have common parameters (for example, σ^2 is common to all models) the difference between the true and the estimated parameters is an obvious measure of performance.

- Likelihood values: The value of the likelihood also gives us an indication of how good the models are fitting the data. Although it is a bit unfair to compare

methods that seek maximizing the likelihood with methods that seek to optimize other criteria, large deviations from the true likelihood should give us an idea of how good the estimated function is.

- Covariance function: Comparing the distance between the true and estimated covariance function or spectral densities seems to be an obvious and esthetically pleasing way of assessing the performance of methods. We use the $\mathcal{L}^2$-norm between the true and estimated covariance function as a measure of performance.

- Prediction performance measures: In most applications, the ultimate goal of estimating the covariance functions is the prediction of the random field at unobserved locations. In this context the $\mathcal{L}^2$-norm can be a misleading benchmark as illustrated by Stein (1999) pg. 66. Following Stein (1999) pg. 58, we define two quantities that are more useful for interpolation purposes. Let $\hat{Z}_i(\mathbf{x})$ be the predicted value at location $\mathbf{x}$ using covariance function C_i and let $e_i(x) = Z(x) - \hat{Z}_i(x)$ be the prediction error; E_i and E_0 are the expectations under the estimated covariance function C_i and under the true covariance function C_0, respectively. With this notation, $E_0 e_0^2$ is the mean squared prediction error (MSPE) of the best linear unbiased predictor or the kriging variance as in Stein (1999) pg. 8 eq. (11), which is computed using the true covariance function; $E_i e_i^2$ is the estimated prediction variance (EPV) computed by plugging in the estimated covariance function C_i in the usual kriging variance; and $E_0 e_i^2$ is the actual variance of the prediction error. It is easy to show that

$$E_0 e_i^2(x)/E_0 e_0^2(x) = 1 + E_0(\hat{Z}_i(x) - \hat{Z}_0(x))^2/E_0 e_0^2(x). \qquad (17)$$

We estimate the numerator on the right side of (17) by computing the sample mean (over 100 simulations and 200 replications in time) of the squared difference between the interpolated values with the misspecified covariance function

and the interpolated values with the true covariance function:

$$\frac{1}{200}\frac{1}{100}\sum_{\text{simul.}}^{100}\sum_{\text{repl.}}^{200}(\hat{Z}_i(x)-\hat{Z}_0(x))^2.$$

So the prediction performance measures we use are:

- The increase in Prediction Error, IPE($\mathbf{x}$), is the second term on the right hand side of (17) and represents the extra mean squared prediction error incurred by using estimated (misspecified) covariance function instead of the true covariance function.

- The Log Variance Ratio, LVR(x) $= |\log(E_i e_i^2(\mathbf{x})/E_0 e_i^2(\mathbf{x}))|$, is the ratio between the estimated and actual variance of the prediction error at location $\mathbf{x}$.

For testing, we use 100 prediction locations on a square grid inside the observation region. The median of IPE and LVR over the prediction locations are used as performance measures.

Table 1 shows the average results of running 100 simulations for each of the following models: Matérn ($\nu = 3$, $\phi = 9.4$), polynomial Matérn ($\nu = 3$, $\phi = 9.4$, $u = 4.7$, $v = 0.94$), S+T ($\nu = 3$, $w_t = 9.4$, $l = 4$, $\mathbf{b} = (1, 0.2, 2, 0.6, 0.4)$), and spectral exponential ($\phi = 9.4$). For all the models $\sigma^2 = 1$, and the unit for ϕ and w_t is $1/1000$ km.

The first three rows show the smoothness parameters, true and estimated, using the S+T and Matérn models. When the true model is Matérn or polynomial Matérn, the estimated smoothness for the S+T model is around 2.2, a bit smaller than the truth, which was 3. This is expected for the Matérn model, since the rate of decay of the estimating tail function $1/w^{2\nu+2}$ is faster than the rate of decay of the true tail function $1/(a^2 + w^2)^{\nu+1}$. We can see this more clearly by comparing the derivatives

16

of the logs of the two tail functions

$$-\frac{2\nu + 2}{w} \quad \text{vs.} \quad -\frac{2(\nu + 1)w}{a^2 + w^2} = -\frac{2\nu + 2}{w} + \frac{2a^2(\nu + 1)}{w(w^2 + a^2)},$$

or more clearly

$$\nu \quad \text{vs.} \quad \nu - \frac{a^2(\nu + 1)}{w^2 + a^2}. \tag{18}$$

Hence the estimated power should be smaller in absolute value than the true power. The estimation process will try to match the left and right side of (18) in an average sense. A similar argument works for the polynomial Matérn function.

When simulating under the S+T model, there is no approximation in the tail, and the S+T model gives an estimated value that is very close to the truth. In the case of the spectral exponential model, we do not have a true parameter with which to compare. We notice that S+T and Matérn methods give similar estimates of the smoothness when the true model is spectral exponential.

When the true models are polinomial Matérn and S+T, the Matérn method yields very large estimates for smoothness, 10 and 7.47, respectively. The comparison with the S+T method may seem a bit unfair since for the latter we have restricted the smoothness parameter to be smaller than 5. But when we restricted the Matérn's smootheness to be smaller than 5, the estimated smoothness was exactly 5 for all 100 simulations and we found no substantial change in the performance of the method. So the thresholding of the smoothness had no effect in the advantage of our method over the Matérn.

The estimated values of the sill (σ^2) are very close to the true value of 1 for all three methods except for the Matérn method when the true model is S+T, which yields a mean of 1.15 with standard deviation 0.03, and the kernel method when the truth is spectral exponential, which yields a mean of 0.97 with standard deviation 0.01. The S+T method gives 1.00 with error 0.02 when the true model is Matérn,

polynomial Matérn and S+T. When the true model is spectral exponential, we get 1.00 with standard deviation 0.01.

The next two blocks of rows show the cutoff frequency w_t and the inverse range. For the S+T model, the average estimated value of w_t is 10.6 (in 1/1000km units) with standard deviation 1.4, compared to true value of 9.4. For the Matérn model the average estimated inverse range parameters are 9.4 with a standard deviation of 0.3.

The $\mathcal{L}^2$-norm between the true and estimated covariance functions are shown next. The S+T method is better by factors of 2.3, 2.8, 2.8 and 1.8 compared to the kernel method when the true models are Matérn, polynomial Matérn, S+T, and spectral exponential, respectively. The S+T method also gives smaller $\mathcal{L}^2$-norm compared to Matérn method except when the Matérn model is the truth. The $\mathcal{L}^2$-norms were calculated by averaging the squared differences between the true and estimated covariance function values at 100 equispaced points in the range 0 to $r_{\max}$.

The last block shows the log likelihood ratio between alternative models and the S+T model. The S+T model gives larger likelihood in all cases except when we use the Matérn model to estimate and the data were simulated from the Matérn model. Even then, the advantage of using the correct parametric model is modest.

Table 2 shows the prediction performance measures of each method. The first three rows compare the median IPE, the increase in MSPE by using estimated covariance function instead of the truth.

The IPEs of the predictors using the S+T method are less than 0.2% for all four simulated models. Namely, the increases are only 0.16%, 0.12%, 0.05%, and 0.12%. The kernel method gives prediction errors 17.5%, 3.8%, 68.5% and 0.3% higher than the best linear predictor while the Matérn method gives errors 0.01%, 1.8%, 4.2% and 0.4% higher. The next three rows compare the LVR, log ratios of the estimated

(via plug in) and the actual variances of the prediction error.

Our method gives EPVs that differ by about half a percent from the actual prediction variance. As a comparison, the kernel method gives EPVs that differed from the actual prediction variance by 59.1%, 27.0%, 100.8% and 5.8% for the four models, and the Matérn method's differences were 0.3%, 0.9%, 8.3%, and 1.2%, both substantially worse than the S+T method except for the Matérn method when the truth is Matérn.

We plotted (not shown in the paper) the smoothed difference between the MSPE of the S+T and the other two methods vs. the minimum distance to observations. In all cases except when the true model was Matérn, our method yielded smaller MSPEs than the other two for all distances. Most of the times the kernel method performed substantially worse than the other two methods. For the polmatern and S+T models, the difference between our method and Matérn increased with distance, which has a natural connection with the fact that our method gives better fit at small frequencies for all simulated models. In contrast, the difference with kernel method decreased with distance. We attribute this fact to the inability of the kernel method to capture the high frequency properties of the spectral density. When the true model was spectral exponential the performance of all three methods was very good since their IPE was less than 1% but we found no obvious pattern in the differences as functions of distance.

We have done simulation studies for other parameter values with qualitatively similar results. In practice, we often need to estimate the mean. When the mean is unknown, we can use restricted likelihood to estimate the parameters, and the simulation results are very similar to the case when the mean is assumed known. These numerical results can be found in Im (2005) and are not presented here.

Figures 2 - 5 show the covariance function (left) and the spectral density (right)

for the Matérn, polynomial Matérn, S+T, and spectral exponential models. These figures show one typical simulation from each model. As suggested by the $\mathcal{L}^2$-norm values from Table 1, the covariance functions estimated using S+T method are closer to the true covariance functions than the kernel estimators. The kernel estimator of the covariance function becomes wiggly for large distances, mainly because there are fewer pairs of observations that contribute to this region. The right sides of Figures 2 - 5 show that our method yields estimates of the spectral densities that are quite close to the truth except near the origin. The Matérn method is not able to reproduce the structure of the spectral density at low and mid frequencies, but it captures reasonably well the tail behavior. The kernel estimates of the spectral density follow the overall shape of the function, but they are very wiggly. We also see several intervals of frequencies where the kernel estimator takes value 0, which is due to the truncation of the function necessary to ensure positive definiteness of the corresponding covariance function. When we calculated the spectral density, we followed the ad hoc solution proposed by Hall et al. (1994): from some point T_1 use a straight line that goes from the value of the estimator at T_1 to zero at some other distance T_2. We chose $T_1 = 1500$km and $T_2 = 2000$km. The actual transformation was done using the fast Hankel transform method proposed by Siegman (1977).

5   Application to rainfall data

In this section we applied the three aforementioned methods to an annual rainfall dataset in the eastern US to compare their performance in prediction. We chose the study region to be between latitudes 27.1 and 49.0 and longitudes -100.5 and -80.2, which includes 2742 stations (dots on the right of Figure 1). The time period of the data is between 1960 and 1999. Detailed documentation of this dataset can be found at http://www1.ncdc.noaa.gov/pub/data/documentlibrary/tddoc/td9651.pdf.

We used 2082 stations that had no missing data. For each station data we subtracted the mean over the 40 years of data and modeled the difference as a Gaussian random process. We looked at the normal quantile plots of the difference for all the stations at each year, and in most of the years the data are consistent with the Gaussian assumption. Some of those normal quantile plots appear to have a few large outliers. The number of possible outliers are never larger than 0.5% of the stations. No attempts were made to identify those outliers. Instead we used robust measures to compare the three methods. An examination of the autocorrelation and cross correlation of the observations at different stations reveals no significant time dependence, thus we model the observations from each year as independent realizations of the same process with a different mean. The empirical variogram suggested the need to include a nugget term in the covariance model. This is straightforward for the two likelihood methods (S+T and Matérn). The kernel method needs some modification in order to handle the nugget effect. One possible way is to estimate the covariance function using only distinct pairs, i.e., $(Z_i - \bar{Z})(Z_j - \bar{Z})$ with $i \neq j$. This leaves out the nugget term. We estimate the nugget by subtracting the estimated covariance function at zero from the sample variance.

We randomly chose 200 training stations among 2082 stations to estimate the covariance function using all three methods (S+T, Matérn, and kernel). With the estimated covariance functions, we kriged the data at the remaining 1882 test stations. We repeated this process for 10 different samples of 200 stations. The location of the first sample of 200 stations are shown as "+"'s on the right panel of Figure 1.

We calculated the mean over 40 years of the prediction error $\mathrm{MPE}(x) = \sqrt{\sum_{t=1}^{40} (Z(\mathbf{x}) - \hat{Z}_i(\mathbf{x}))^2/40}$ and an empirical estimate of the LVR as $|\log(\mathrm{MPE}^2(x)/\mathrm{EPV}(x))|$. Table 3 shows the median over locations and samples of the MPEs and LVRs. Our method yields on average 1.5% better prediction errors than the kernel method.

The LVR of our method is about 4% better than the kernel method. There is no noticeable difference in performance between our method and Matérn. The estimated spectral density using ourmethod did not show any interesting structure in the middle freequencies that could be missed by the Matérn spectral function. This could explain the lack of advantage of using our method.

We have tried using 100 training stations and the results were similar. We plotted (not shown in the paper) smoothed MPEs and LVRs vs. the closest distance to observations and found no obvious pattern.

6   Summary and discussion

In this paper we propose a new method to estimate spectral densities of isotropic Gaussian processes with scattered data using a flexible semiparametric S+T model, whose parameters can be estimated using ML or REML methods. We have calculated explicit expressions of the Hankel transform of the spectral density and tackled several numerical issues arising during the computation of the covariance function. Simulated annealing is used to maximize the likelihood.

To compare our method with other existing method for estimating spectral density, we simulated observations with Matérn, polynomial Matérn, S+T, and spectral exponential spectral densities. Our simulation results showed that our method (S+T) outperforms the non-parametric kernel method in terms of estimated sill, $\mathcal{L}^2$-norms of the covariance functions, the likelihood values, MSPE, and errors in the estimated variances of the predictions. Our method also outperforms the parametric method using the Matérn covariance model when the true model is not Matérn by all these performance criteria. All three methods are applied to a rainfall data to compare the prediction performance, with our method doing better than the kernel method and as well as the Matérn method.

The IPEs and the LVRs are the most relevant measures of performance when our ultimate goal is interpolation to locations where there are no observations. With this criteria, the Matérn method outperforms the kernel method, although it generally has larger $\mathcal{L}^2$-norm values of the covariance function than the kernel method when the truth is not Matérn. The reason for the better prediction properties of the Matérn method is that the tail properties of the spectral function play a fundamental role in the prediction. This result point out the inefficiency of methods that rely on minimizing the distance to empirical variograms such as kernel method

Our method does well because it directly estimates the tail property just like the Matérn method does, while it also offers more flexibility for modeling the lower frequencies. A point to note is that our method outperforms the kernel method even when the true model is spectral exponential, which has an exponential tail, whereas our method assumes an algebraic tail.

We have performed simulations with smaller number of replicates (20 and 1 instead of 200 of the 63 sites) per simulation. Using the prediction performance criteria, we found that our method outperforms the Matérn method when the number of replicates is 20, but not so when we only have one replicate of the spatial process. So our method should be applied with caution when one does not have a large amount of data.

We applied all three methods to 40 years of annual rainfall data in the Eastern US and showed that our method outperforms the kernel method in terms of prediction error and estimated uncertainty. However, we did not find any noticeable difference in performance between our method and the Matérn method when applied to this dataset. We may need to look for a dataset with a more comlex middle frequency structrure in order to see an advantage of using our method.

In this work we used equally spaced nodes for the B-splines and did not attempt to estimate the optimal spacing of the nodes. Our method can be modified to allow

the spacing of the nodes to be estimated from the data. One possible way of doing this efficiently is to utilize the information contained in the kernel estimator. Even though the kernel method fails to capture the tail behavior of the spectral density, it does seem to have useful information about the mid frequency shape of the function. We plan to address this possibility in a separate paper.

One interesting extension of our work would be to use transdimensional markov chains, such as reversible jump Markov Chains, to optimize over both parameter and number and location of nodes. Although some form of regularization is built into our model through the smoothness of the B-splines and the algebraic tail, we may need to consider Tychanoff's regularizations or a prior distribution that discourages large number of knots when using the Markov Chain approch.

Acknowledgements

References

Abramowitz, M. and Stegun, I. (1965), *Handbook of Mathematical Functions*, New York: Dover, 9th ed.

Akaike, H. (1974), "A new look at the statistical identification model," *IEEE Transactions on Automatic Control*, 19, 716–723.

de Boor, C. (2001), *A Practical Guide to Splines*, Springer.

Genton, M. G. and Gorsich, D. J. (2002), "Nonparametric variogram and covariogram estimation with Fourier-Bessel matrices," *Computational statistics & Data Analysis*, 41, 47–57.

Givens, G. H. and Hoeting, J. A. (2005), *Computational Statistics*, Wiley.

Hall, P., Fisher, N., and Hoffmann, B. (1994), "On the nonparametric estimation of covariance functions," *Annals of Statistics*, 22, 2115–2134.

Handcock, M. S. and Wallis, J. R. (1994), "An approach to statistical spatial temporal modeling of meteorological fields," *Journal of the American Statistical Association*, 89, 368–378.

Im, H. K. (2005), "Two problems in environmetrics," Ph.D. thesis, University of Chicago, http://galton.uchicago.edu/~stein.

McCullagh, P. and Nelder, J. A. (1989), *Generalized Linear Models*, London: Chapman and Hall, 2nd ed.

Schwarz, G. (1978), "Estimating the dimension of a model," *The Annals of Statistics*, 6, 461–464.

Shapiro, A. and Botha, J. D. (1991), "Variogram fitting with a genral class of conditionally nonnegative definite functions," *Computational Statistics & Data Analysis*, 11, 87–96.

Siegman, A. E. (1977), "Quasi fast Hankel transform," *Optics Letters*, 1, 13–15.

Stein, M. L. (1999), *Statistical Interpolation of Spatial Data: Some Theory for Kriging*, New York: Springer.

— (2002), "The screening effect in kriging," *Annals of Statistics*, 30, 298–323.

Wolfram Research,Inc. (2001a), "Gamma function," `http://functions.wolfram.com/Gamma`.

— (2001b), "Gamma function," `http://functions.wolfram.com/GammaBetaErf/PolyGamma`.

— (2001c), "Generalized Hypergeometric Function $_1F_2$," `http://functions.wolfram.com/HypergeometricFunctions/Hypergeometric1F2/`.

Yaglom, A. M. (1987), *Correlation Theory of Stationary and Related Random Functions*, vol. 1, New York: Springer-Verlag.

Appendix

A B-splines

The following is a summary of the properties of B-splines relevant for this work. For a more extensive description see de Boor (2001).

A piecewise polynomial of order k with strictly increasing break (node) sequence ξ is a function of the form

$$\sum_j \mathbf{1}_{[\xi_j, \xi_{j+1})} p^{(k)}(x) \tag{19}$$

where $p^{(k)}(x)$ is a polynomial of degree $k - 1$ or smaller. The set of all piecewise polynomial functions of order k with break sequence ξ is denoted $\Pi_{<k,\xi}$.

B-splines are defined in terms of a non-decreasing knot sequence $\mathbf{t} = (t_j)$. The jth B-spline of order 1 for knot sequence $\mathbf{t}$ is the indicator function of the interval $[t_j, t_{j+1})$:

$$B_{j,1} := B_{j,1,\mathbf{t}} = \mathbf{1}_{[t_j, t_{j+1})}. \tag{20}$$

If $t_j = t_{j+1}$, $B_j = 0$. The jth B-spline of order $k > 1$ is defined by the following recurrence relation

$$B_{jk} := B_{j,k,\mathbf{t}} := w_{jk} B_{j,k-1} + (1 - w_{j+1,k}) B_{j+1,k-1} \tag{21}$$

with $w_{jk} := w_{j,k,\mathbf{t}} := \frac{x - t_j}{t_{j+1} - t_j}$. B_{jk} is a piecewise polynomial function with break sequence $t_k, ..., t_{j+k}$. It is positive on $[t_j, t_{j+k}]$ and 0 outside this interval. B-splines of order k with knot sequence $\mathbf{t}$ span the space of piecewise polynomial functions of order k with break sequence ξ and continuity conditions on the breaks given by the multiplicity of the knots. More specifically, the sum of the number of continuity conditions at a break ξ_j and the number of repeated knots at ξ_j equals the order k.

For the uniform knot sequence $t = (..., -\Delta, 0, \Delta, 2\Delta, ...)$ the corresponding B-splines are

$$B_{j,k,\mathbf{t}}^{\Delta}(x) = \sum_{r=0}^{k} \frac{(-1)^{k-r}}{(k-1)!} \binom{k}{r} (r - x/\Delta + j)_+^{k-1} \tag{22}$$

In particular, for $k = 4$, $j = 0$, and $\mathbf{t} = \mathbb{Z}$ and $\Delta = 1$

$$B(x) := B_{0,4,\mathbb{Z}}^{1}(x) = \begin{cases} x^3/6 & \text{if } 0 \le x < 1; \\ (-3x^3 + 12x^2 - 12x + 4)/6 & \text{if } 1 \le x < 2; \\ (3x^3 - 24x^2 + 60x - 44)/6 & \text{if } 2 \le x < 3; \\ (-x^3 + 12x^2 - 48x + 64)/6 & \text{if } 3 \le x < 4; \end{cases} \tag{23}$$

For arbitrary Δ and $j \ne 0$ the B-splines are obtained from (23) by translating the argument by $j\Delta$ and scaling it by $1/\Delta$, i.e., $B_{j,4,\mathbb{Z}}^{\Delta}(x) = B_{0,4,\mathbb{Z}}^{1}(\frac{x - j\Delta}{\Delta})$.

B Hankel transform of polynomials

The Hankel Transforms of piecewise polynomials of the form $(w - c)^m$ are given by

$$\int_{a'}^{b'} (w - k')^m w J_o(wr) dw = r^{-m-2} \int_{a'r}^{b'r} u(u - k'r)^m J_o(u) du, \tag{24}$$

which for $a = a'r$, $b = b'r$, $k = k'r$, and $m = 0, 1, 2,$ and 3 are

$$\int_a^b u J_o(u) du = -a J_1(a) + b J_1(b),$$

$$
\begin{aligned}
\int_a^b (u - k) u J_o(u) du =\ & J_1(a)(-a^2 + a(k + (\pi H_o(a))/2)) + J_1(b)(b^2 + b(-k - (\pi H_o(b))/2)) \\
& -(a\pi J_o(a) H_1(a))/2 + (b\pi J_o(b) H_1(b))/2,
\end{aligned}
$$

$$
\begin{aligned}
\int_a^b (u - k)^2 u^2 J_o(u) du =\ & J_1(a)(-a^3 + 2a^2 k + a(4 - k^2 - k\pi H_o(a))) + J_o(a)(-2a^2 + ak\pi H_1(a)) \\
& + J_1(b)(b^3 - 2b^2 k + b(-4 + k^2 + k\pi H_o(b))) + J_o(b)(2b^2 - bk\pi H_1(b)),
\end{aligned}
$$

and

$$
\begin{aligned}
\int_a^b (u - k)^3 u J_o(u) du =\ & J_1(a)(-a^4 + 3a^3 k + a^2(9 - 3k^2) + a(-12k + k^3 + (-9/2 + (3k^2)/2)\pi H_o(a))) \\
& + J_1(b)(b^4 - 3b^3 k + b^2(-9 + 3k^2) + b(12k - k^3 + (9/2 - (3k^2)/2)\pi H_o(b))) \\
& + J_o(a)(-3a^3 + 6a^2 k + a(9/2 - (3k^2)/2)\pi H_1(a)) \\
& + J_o(b)(3b^3 - 6b^2 k + b(-9/2 + (3k^2)/2)\pi H_1(b)),
\end{aligned}
$$

where $J_\nu(\cdot)$ are Bessel functions of the first kind of order ν and $H_\nu(\cdot)$ are Struve functions of order ν (Abramowitz and Stegun, 1965).

C Continuity of derivative

For uniform knots with spacing Δ, the values of the spectral density on (w_{n-1}, w_n) where $w_n = \Delta n = w_t$ is

$$f(w) = f_n B\left(\frac{w - w_{n-2}}{\Delta}\right) + f_{n-1} B\left(\frac{w - w_{n-3}}{\Delta}\right) + f_{n-2} B\left(\frac{w - w_{n-4}}{\Delta}\right) + f_{n+1} B\left(\frac{w - w_{n-1}}{\Delta}\right). \tag{25}$$

It follows that

$$f'(w) = f_n B'(\frac{w - w_{n-2}}{\Delta}) + f_{n-1}B'(\frac{w - w_{n-3}}{\Delta}) + f_{n-2}B'(\frac{w - w_{n-4}}{\Delta}) + f_{n+1}B'(\frac{w - w_{n-1}}{\Delta}).$$

At $w = w_t$, $f'(w_t) = -\frac{nf_{n-1}}{2w_n} + \frac{nf_{n+1}}{2w_t}$. If we want $f'(w)$ to be continuous at w_t, we

need $f'(w_t) = -\frac{\gamma f_t}{w_t}$, where $f_t = \frac{1}{6}f_{n-1} + \frac{2}{3}f_n + \frac{1}{6}f_{n+1}$. Thus we have

$$f_{n+1} = \frac{3n - \gamma}{3n + \gamma}f_{n-1} - \frac{4\gamma}{3n + \gamma}f_n. \tag{26}$$

D   Positivity of the spectral density

Our model allows the values of the $(n+1)^{\text{th}}$ coefficient to be negative, and we need

to check whether the spectral density is still positive on the interval $(0, w_t)$. Because

of the linearity of the derivative, it is enough to consider separately the cases where

$f_n = 0$ and $f_{n-1} = 0$. If we get positive spectral density in each case the sum of

the two will also result in a positive function. Also, since the support of the B-spline

with coefficient f_{n+1} (B) is (w_{n-1}, w_{n+3}), we only need to worry about the interval

(w_{n-1}, w_n).

Case $f_{n-1} = 0$

Since each of the terms in (25) is nonnegative except possibly for the term corre-

sponding to f_{n+1}, we have

$$f(w) \geq f_n B(x) + f_{n+1}B(x - 1) := g(x), \tag{27}$$

where $x = \frac{w - w_{n-2}}{\Delta}$. To show $f(w) \geq 0$ for $w \in (w_{n-1}, w_n)$, it is enough to show

$g(x) \geq 0$ for $x \in (1, 2)$. Substituting the corresponding piecewise polynomial in each

case and using (26), we get

$$\begin{aligned} g(x) &= \frac{f_n}{6}\left(-3x^3 + 12x^2 - 12x + 4 - \frac{4\gamma}{3n + \gamma}(x - 1)^3\right) \\ &= \frac{f_n}{6}\left(\frac{2\gamma + 3n}{2(3n + \gamma)}(2 - x)(4 - 10x + 7x^2) + \frac{3n}{2(3n + \gamma)}x^3\right). \end{aligned} \tag{28}$$

29

Since $4 - 10x + 7x^2 > 0$, it follows that $g(x) \geq 0$ for $x \in (1, 2)$.

Case $f_n = 0$

We have

$$f(w) \geq f_{n-1}B(x) + f_{n+1}B(x - 2) := g(x), \tag{29}$$

where $x = \frac{w - w_{n-3}}{\Delta}$, and $x \in (2, 3)$ for $w \in (w_{n-1}, w_n)$. To show $g(x) \geq 0$ for $x \in (2, 3)$, we next show that the function $g(x)$ is monotone decreasing and that the value at $x = 3$ is positive. Since

$$g(x) = \frac{f_{n-1}}{6} \left(3x^3 - 24x^2 + 60x - 44 + \frac{3n - \gamma}{3n + \gamma}(x - 2)^3 \right), \tag{30}$$

we have $g(3) = f_{n-1}\frac{n}{3n+\gamma} > 0$, and

$$g'(x) = 6f_{n-1}\frac{(x - 2)(\gamma(x - 4) + 6n(x - 3))}{3n + \gamma} \leq 0 \tag{31}$$

for $x \in (2, 3)$. Thus $g(x) > 0$ for $x \in (2, 3)$

E   Tail integral with integer smoothness

Using the series representation of the hypergeometric function, the integral of the tail given in (11) can be written as

$$\int_{s_t}^{\infty} u^{1-\gamma} J_o(u) du = \frac{(-\gamma/2)\Gamma(-\gamma/2)}{2^{\gamma-1}\Gamma(-\gamma/2)} + \frac{s_t^{2-\gamma}}{\gamma - 2} \sum_{k=0}^{\infty} \frac{-\gamma/2 + 1}{-\gamma/2 + 1 + k} \frac{(-st^2/4)^k}{k!^2}. \tag{32}$$

Let $-\gamma/2 + 1 = -n + \delta$ with $n \in \mathbb{N}$. As δ goes to zero, the first term in (32) and the nth term in the second term of (32) go to infinity but the total contribution of the diverging terms is finite. This can be shown by using the asymptotic expansion of the gamma function when the argument is close to a negative integer. We reorder the

terms in (32) to make explicit the two terms that diverge when $\gamma/2$ is integer valued:

$$\int_{s_t}^{\infty} u^{1-\gamma} J_o(u)du = \frac{\Gamma(-n+\delta)}{2^{\gamma-1}\Gamma(n+1-\delta)} + \frac{s_t^{2-\gamma}}{\gamma-2} \frac{-n+\delta}{\delta} \frac{(-st^2/4)^n}{n!2} +$$
$$+ \frac{s_t^{2-\gamma}}{\gamma-2} \sum_{k=0,k\neq n}^{\infty} \frac{-\gamma/2+1}{-\gamma/2+1+k} \frac{(-st^2/4)^k}{k!2}. \tag{33}$$

Using $\Gamma(-n+\delta) = \frac{(-1)^n}{n!\delta} + \frac{(-1)^n \psi(n+1)}{n!} + O(\delta)$ (Wolfram Research,Inc., 2001a), where $\psi(n+1)$ is the digamma function (Wolfram Research,Inc., 2001b), we get

$$\int_{s_t}^{\infty} u^{1-\gamma} J_o(u)du = -\frac{2^{-1-2n} s_t^{2(\delta-n)} \left(-s_t^2\right)^n}{\delta\,n!2} - \frac{(-1)^n\, 2^{-1+2\delta-2n}}{\delta\,n!\,\Gamma(1-\delta+n)}$$
$$+ \frac{(-1)^n\, 2^{-1+2\delta-2n}\,\psi(0,1+n)}{n!\,\Gamma(1-\delta+n)} + \sum_{k=0,k\neq n}^{\infty} \ldots + O(\delta). \tag{34}$$

By letting δ go to zero, we have

$$\int_{s_t}^{\infty} u^{1-\gamma} J_o(u)du = \frac{\log(2) - \log(s_t) + \psi(n+1)}{(-4)^n n!2} + \frac{s_t^{2-\gamma}}{\gamma-2} \sum_{k=0,k\neq n}^{\infty} \frac{-\gamma/2+1}{-\gamma/2+1+k} \frac{(-s_t^2/4)^k}{k!2}. \tag{35}$$

F   Asymptotic expansion of tail

We use the following asymptotic expansion of $_1F_2$ for large z to find an approximate expression for the truncated tail integral.

$$_1F_2(a_1; b_1, b_2; z) \approx \frac{\Gamma(b_1)\,\Gamma(b_2)\,(-z)^{a_1}}{\Gamma(-a_1+b_1)\,\Gamma(-a_1+b_2)} \left(1 + \frac{a_1\,(1+a_1-b_1)\,(1+a_1-b_2)}{z}\right.$$
$$+ \frac{a_1\,(1+a_1)\,(1+a_1-b_1)\,(2+a_1-b_1)\,(1+a_1-b_2)\,(2+a_1-b_2)}{2\,z^2} + \ldots \Big)$$
$$+ \frac{(-z)^\chi\,\Gamma(b_1)\,\Gamma(b_2)}{2\sqrt{\pi}\,\Gamma(a_1)} \left(\cos\left(2\sqrt{-z}+\pi\chi\right)\left(1+\frac{d_2}{z}+\ldots\right) + \sin\left(2\sqrt{-z}+\pi\chi\right)\left(\frac{d_1}{\sqrt{-z}}+\ldots\right)\right) \tag{36}$$

for large z (Wolfram Research,Inc., 2001c), where

$$\chi = \frac{1}{2} \left(\frac{1}{2} + a_1 - b_1 - b_2 \right),$$

$$d_1 = \frac{1}{16} \left(-3 + 12\,a_1{}^2 - 4\,b_1{}^2 + 8\,b_2 - 4\,b_2{}^2 + 8\,b_1\,(1 + b_2) - 8\,a_1\,(1 + b_1 + b_2) \right),$$

$$d_2 = \frac{1}{512} \left(-15 + 144\,a_1{}^4 + 16\,b_1{}^4 + 16\,b_2 + 56\,b_2{}^2 - 64\,b_2{}^3 + 16\,b_2{}^4 \right.$$

$$-64\,b_1{}^3\,(1 + b_2) - 64\,a_1{}^3\,(7 + 3\,b_1 + 3\,b_2) + 8\,b_1{}^2\,\left(7 + 8\,b_2 + 12\,b_2{}^2 \right)$$

$$+16\,b_1\,\left(1 + 25\,b_2 + 4\,b_2{}^2 - 4\,b_2{}^3 \right) - 8\,a_1{}^2\,\left(-43 + 4\,b_1{}^2 - 72\,b_2 + 4\,b_2{}^2 - 8\,b_1\,(9 + 5\,b_2) \right)$$

$$\left. +16\,a_1\,\left(-1 + 4\,b_1{}^3 - 25\,b_2 - 4\,b_2{}^2 + 4\,b_2{}^3 - 4\,b_1{}^2\,(1 + b_2) - b_1\,\left(25 + 40\,b_2 + 4\,b_2{}^2 \right) \right) \right).$$

Substituting this expression for $_1F_2$ in (11) and we have (13) for $wr \to \infty$.

			Truth		
		Matérn	polMatérn	S+T	spect. exp'l
	true	3	3	3	–
ν	S+T	2.15 (0.10)	2.21 (0.26)	3.00 (0.06)	1.82 (0.70)
	Mat	2.98 (0.09)	10.00 (2.39)	7.47 (0.31)	1.63 (0.18)
	true	1	1	1	1
	S+T	1.00 (0.02)	1.00 (0.02)	1.00 (0.02)	1.00 (0.01)
σ^2	Mat	1.00 (0.02)	1.00 (0.02)	1.15 (0.03)	1.00 (0.01)
	Ker	0.99 (0.03)	0.98 (0.02)	0.99 (0.02)	0.97 (0.01)
	true	–	–	9.4	–
$w_t \times 1000$	S+T	12.3 (1.2)	18.7 (2.1)	10.6 (1.4)	32.7 (5.1)
inv.range	true	9.4	–	–	–
$\times 1000$	Mat	9.4 (0.3)	35.4 (4.6)	15.3 (0.5)	41.0 (195.7)
$\mathcal{L}^2$-norm	S+T	8.7 (4.7)	7.9 (3.9)	7.4 (2.7)	5.2 (1.7)
Cov	Mat	7.4 (5.0)	53.6 (0.3)	123.9 (7.8)	10.4 (16.0)
$\times 1000$	Ker	20.6 (6.7)	21.9 (4.8)	20.9 (6.2)	9.2 (1.6)
loglik	Mat	4 (4)	-181 (22)	-296 (22)	-20 (96)
ratio	Ker	-1093 (167)	-254 (34)	-3173 (246)	-28 (9)

Table 1: Summary of simulation results for $\nu = 3.00$, $\sigma^2 = 1.00$, and inverse range (or w_t) = 9.4(1/1000 km). Maximum likelihood estimation. Average estimates from 100 simulations are shown. Each simulation consisted of 12,600 observations (200 replications of 63 spatially correlated observations). Standard deviations are shown in parentheses. Columns correspond to true models and rows correspond to estimating methods: ML using S+T, ML using Matérn, and kernel. Log-likelihoods are differences from S+T.

		Matérn	polMatérn	S+T	spect. exp'l
$E_0 e_1^2 / E_0 e_0^2 - 1$	S+T	0.16 (0.10)	0.12 (0.05)	0.05 (0.07)	0.12 (0.08)
$E_0 e_2^2 / E_0 e_0^2 - 1$	Mat	0.01 (0.00)	1.77 (3.17)	4.24 (3.17)	0.40 (0.63)
$E_0 e_3^2 / E_0 e_0^2 - 1$	Ker	17.51 (32.30)	4.10 (9.10)	68.54 (118.61)	0.26 (0.45)
$|\log(E_1 e_1^2 / E_0 e_1^2)|$	S+T	0.93 (2.83)	0.39 (0.68)	0.33 (0.52)	0.31 (1.29)
$|\log(E_2 e_2^2 / E_0 e_2^2)|$	Mat	0.30 (0.76)	0.86 (2.28)	8.57 (17.24)	1.21 (2.16)
$|\log(E_3 e_3^2 / E_0 e_3^2)|$	Ker	59.08 (94.75)	27.06 (43.31)	100.78 (157.13)	5.79 (16.41)

Table 2: Simulations as in Table 1. The first block of three rows show the median over 100 prediction locations of IPE, the increase in MSPE by using estimated covariance function instead of the truth. The second block of three rows show the median of the log ratio of the estimated prediction variance (EPV) and the actual prediction variance. In all rows the interquartile range is shown in parenthesis. The values are in percentual units.

	S+T	Matérn	Kernel
median MPE	3.12	3.12	3.16
median $|\log(\text{MPE}^2/\text{EPV})|$	0.50	0.50	0.54

Table 3: Prediction performance comparison for annual rainfall data in the eastern US. We used 10 samples of 200 training stations (randomly chosen) to estimate the covariance function and predicted the values at the remaining 1882 stations. The median over samples and prediction locations of the mean prediction error, MPE, and the empirical log variance ratio, LVR, are shown for each method.
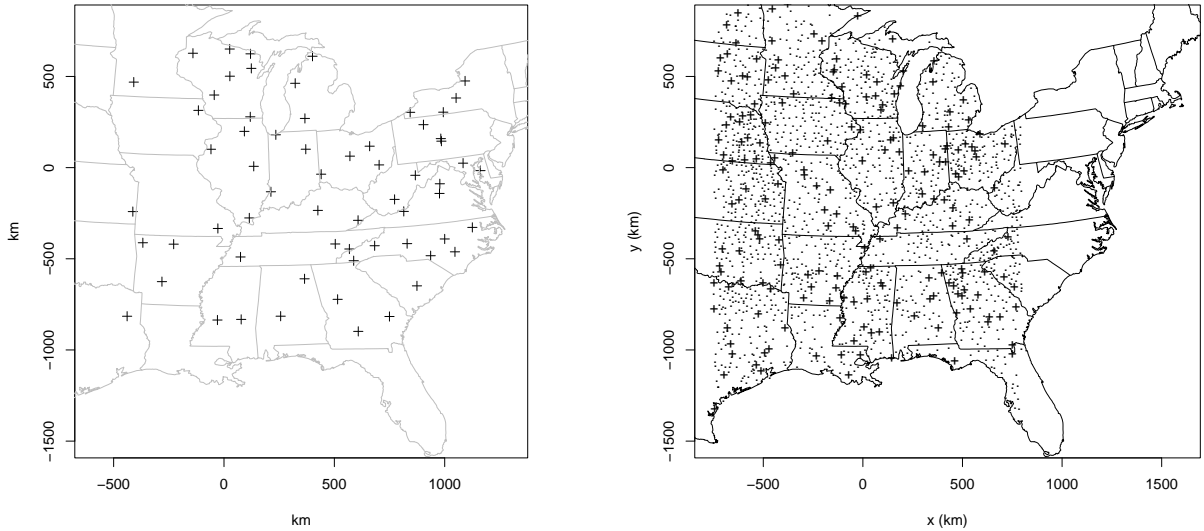
Figure 1: Plot of NADP monitoring sites used for simulations (left), and the monitoring sites for the rainfall dataset (right).
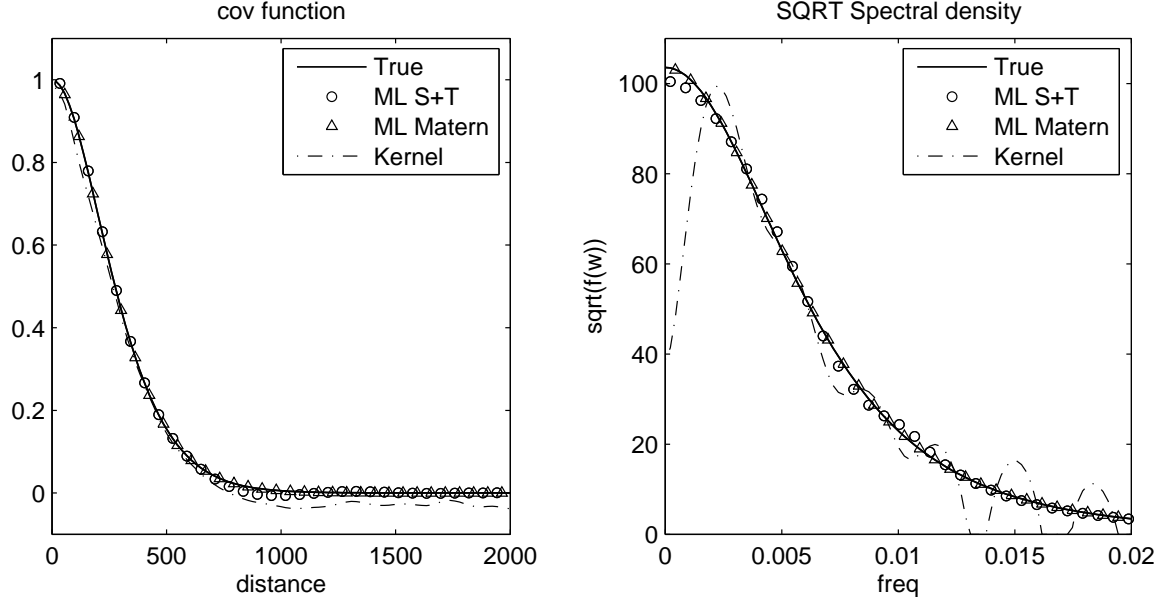
35

Figure 2: True and estimated a) covariance function and b) spectral density. The true model is Matérn with $\nu = 3$, $\sigma^2 = 1.00$, and inverse range $= 9.4$ (1/1000km)
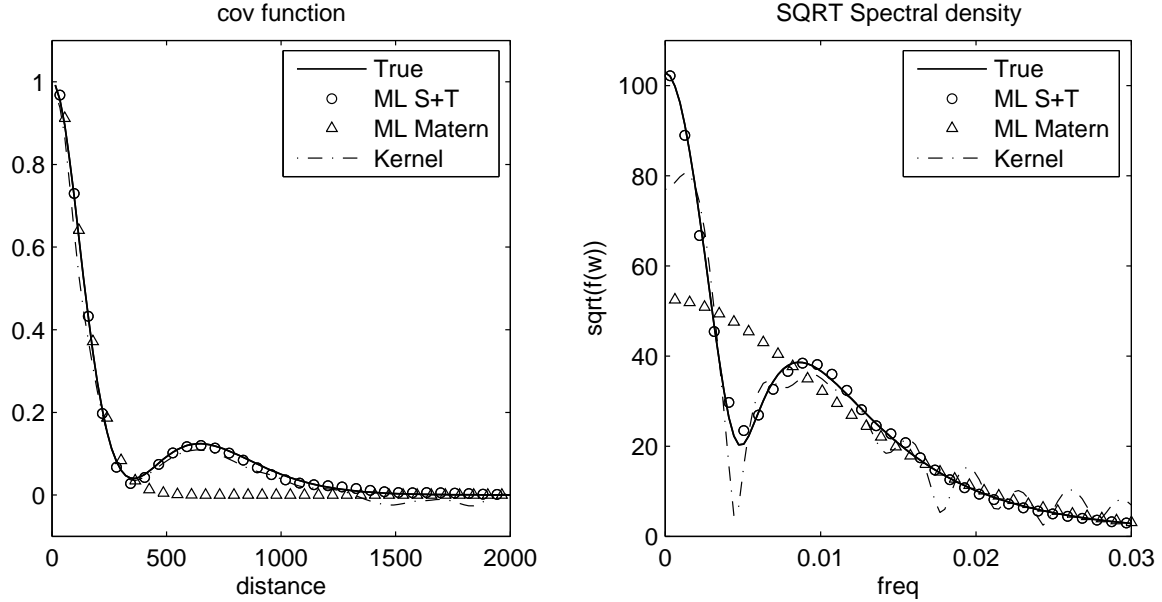

Figure 3: True and estimated a) covariance function and b) spectral density. The true model is polynomial Matérn with $\nu = 3$, $\sigma^2 = 1.00$, inverse range (or w_t) $= 9.4$ (1/1000km), $u = 0.5w_t$, and $v = 0.1w_t$.
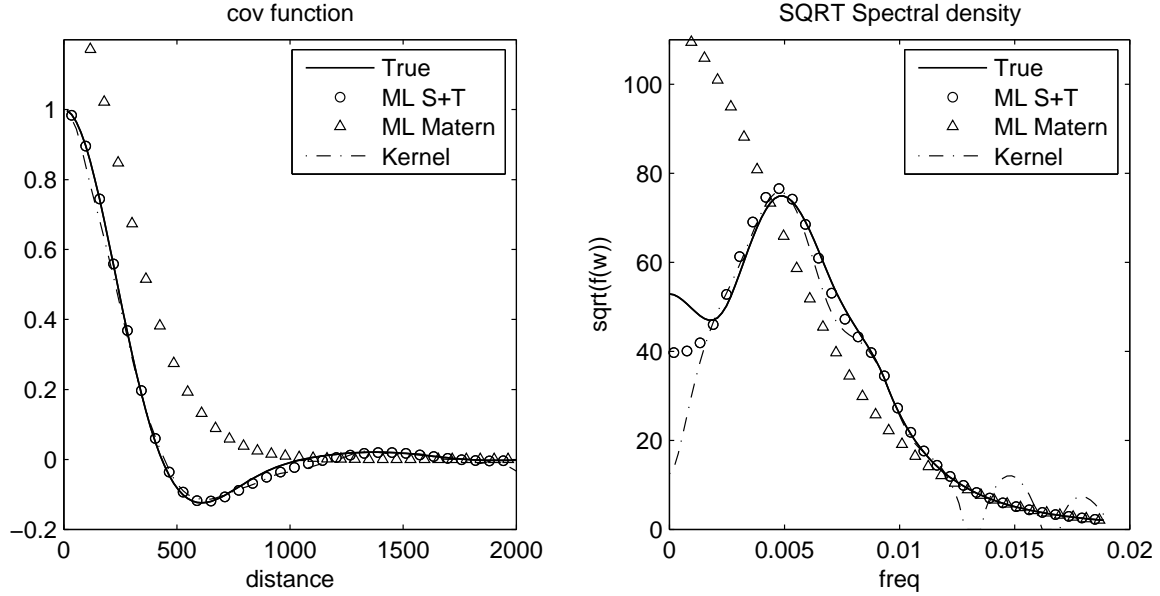
Figure 4: True and estimated a) covariance function and b) spectral density. The true model is S+T with $\nu = 3$, $\sigma^2 = 1.00$, $w_t = 9.4$ (1/1000km), and coefficients $\mathbf{b} = (1, 0.2, 2, 0.6, 0.4)$
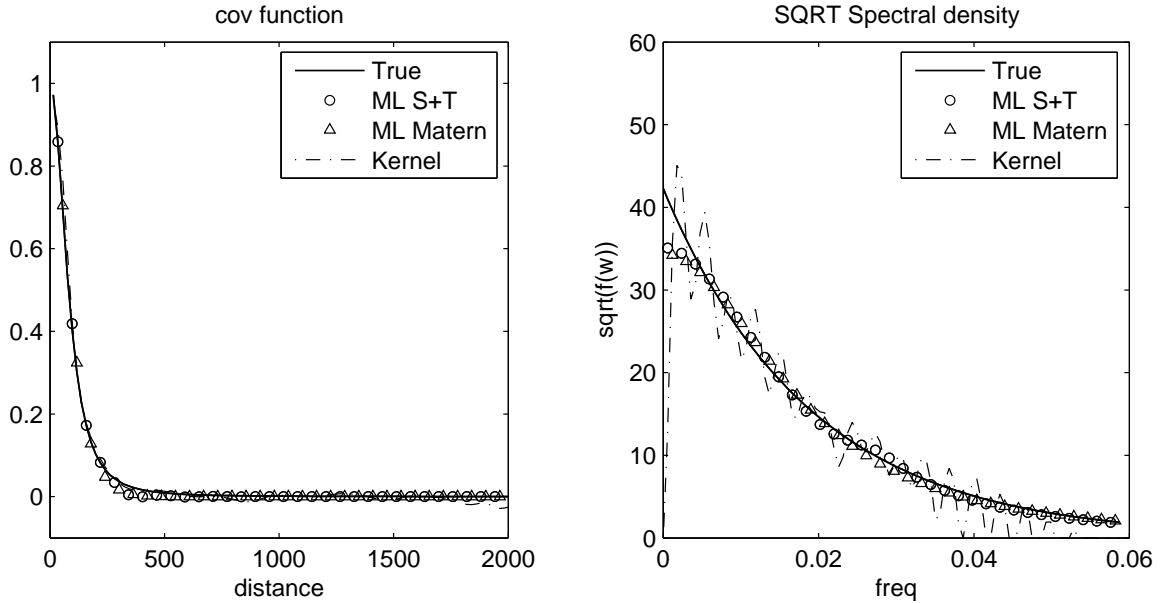

Figure 5: True and estimated a) covariance function and b) spectral density. The true model is spectral exponential with $\sigma^2 = 1.00$ and inverse range = 9.40 (1/1000km)